Czech Technical University in Prague

Faculty of Nuclear Sciences and Physical Engineering

Department of Physical Electronics

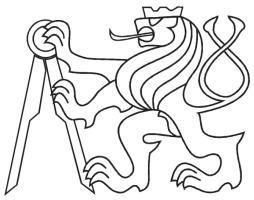

Design and Construction of Fluxgate Magnetometer for Space Research

Bachelor's Degree Project

Author:	Roman Pavelka
Submitted in:	July 2011
Programme:	Engineering Informatics
Branch of Study:	Information Physics
Supervisor:	Ing. Pavel M. Trávníček, Ph.D.
Consultant:	Ing. Josef Blažej, Ph.D.

Prohlášení

Prohlašuji, že jsem svou bakalářskou práci vypracoval samostatně a použil jsem pouze podklady (literaturu, projekty, SW atd.) uvedené v přiloženém seznamu.

V Praze dne ....

Roman Pavelka

Title:

Design and Construction of Fluxgate Magnetometer for Space Research

Author:	Roman Pavelka
Programme:	Engineering Informatics
Branch of Study:	Information Physics
Supervisor:	Ing. Pavel M. Trávníček, Ph.D. Space Plasma Group Astronomical Institute of Czech Academy of Sciences
Consultant:	Ing. Josef Blažej, Ph.D. Faculty of Nuclear Sciences and Physical Engineering Czech Technical University in Prague

Abstract:

The aim of this bachelor thesis is to summarize the general principle of fluxgate magnetometer with relevant physical and engineering knowledge, give an overview of current space-born instruments and design and build simple magnetometer capable of terrestrial measurement of sun-triggered activity of Earth's magnetic field. The design accents low cost, circuit's simplicity, digital implementation and usage of accessible components. Complete description of the manufacturing process is given.

Key words: fluxgate, magnetometer

Název práce:

Návrh a konstrukce fluxgate magnetometru pro vesmírný výzkum

Autor:	Roman Pavelka
Obor:	Inženýrská informatika
Druh práce:	Bakalářská práce
Vedoucí práce:	Ing. Pavel M. Trávníček, Ph.D. Space Plasma Group Astronomický ústav Akademie věd ČR
Konzultant:	Ing. Josef Blažej, Ph.D. Fakulta jaderná a fyzikálně inženýrská České vysoké učení technické

Abstrakt:

Cílem této bakalářské práce je shrnout princip fluxgate magnetometru se souvisejícími fyzikálními a inženýrskými znalostmi, provést rešerši stávajících návrhů používaných na současných výzkumných satelitech a navrhnout a zkonstruovat prototyp přístroje schopného pozemního měření fluktuací zemského magnetického pole způsobených sluneční aktivitou. Návrh klade důraz na nízkou cenu, jednoduchost, digitální zpracování signálu a využití snadno dostupných komponent. Práce je v angličtině a obsahuje kompletní popis postupu výroby.

Klíčová slova: fluxgate, magnetometr

Acknowledgment

I thank my friend Petr Waschinger for helping me to get into the world of microcontrollers, providing me various electronic material, for moral support and for our invaluable technical discussions. Also I would like to thank Jakub Kákona for providing me their great kit MLAB and for sharing his knowledge with others.

I would like to acknowledge Prof. Ing. Pavel Ripka, CSc. for our discussion, which gave me a lot, and for providing me his comprehensive book Magnetic Sensors and Magnetometers. I also appreciate valuable discussion with Ing. Jaroslav Pavel about general electronics design. I thank Pavel Hudeček for insightful advices and his idea to optically interface driving electronics. I'm grateful to Matěj Laitl for his invaluable help with GNU/Linux, especially for introducing me Gentoo distribution and for a plenty of various programming knowledge and tricks, which he taught me. Also I thank Ing. Josef Voltr, CSc. and Ing. David Vyhlídal for their help with microcontroller-peripheries interfacing.

I would like to thank Bc. Adam Winsdor for reading the text, drawing figures 4.2, 4.3 and 4.4, taking all used photographies and teaching me some useful image manipulation tricks. Also I would thank Petr Vála, Bc. Mirek Zima, my father Ing. Roman Pavelka, PhD. and others who read this text and helped me to correct mistakes.

I thank my family for all their support and understanding.

Contents

1 Introduction **6**

2 Goals **7**

3 Physical background **8**
3.1 Magnetic field 8
3.2 Magnetic materials 9
3.3 Transformer 10

4 Principle and basics of fluxgate magnetometers **12**
4.1 Non-linear transformer 12
4.2 Differential measurement 13
4.3 Feedback measurement 15
4.4 Materials for fluxgate sensors 15
4.5 Sensor designs and multi-axial measurement 16

5 Successful instruments, proposed designs and trends **18**
5.1 Ørsted magnetometers 18
5.2 THEMIS magnetometers 20
5.3 Other designs and trends 21

6 Design and prototyping **22**
6.1 Approach 22
6.2 Prototyping 23
6.3 Control unit and communication interface 23
6.4 Drive electronics 25
6.5 Sense electronics 26
6.6 Sensor 27
6.7 Firmware, software and operational procedure 29

7 Testing **32**

8 Conclusion **37**

Bibliography **38**

A Content of enclosed CD-ROM **40**

B Used software **41**

Chapter 1

Introduction

The rapid development and systematization of electromagnetic theory in the 19th century (Maxwell, Faraday, Henry and others) revolutionized most fields of human society. During the 20th century, new military, navigation and research problems arose and precise and accurate measurement of electromagnetic quantities became necessary.

The fluxgate magnetometer is a device developed for precise vector measurement of static magnetic fields. It was invented by Aschenbrenner and Goubau in 1936 and improved during the WWII by Victor Vacquier. It was used for airborne detection of submarines and exploration of mineral and oil deposits. The earliest investigation of outer space environment revealed the importance of research of magnetic fields in the Solar System. Earth's magnetic field was found to be important for terrestrial life because it forms a protective bubble with distinct regions, called magnetosphere, and deflects charged particle flux from the Sun and other extraterrestrial sources. [16] [10]

Further exploration revealed strong coupling of different regions of Earth's magnetosphere to solar activity. Interesting results can be expected from exploring possible connection between terrestrial and space weather. Physics of Earth's magnetosphere became important part of geophysics. Fluxgate magnetometers are very valuable in this field because of their high precision, stability and reliability. [16]

This work studies general principle and current technology of fluxgate magnetometers. Simple digital device was designed and built to monitor local magnetic field variations caused by the solar, human and geological activity. I use available components and digital design to achieve construction and calibration simplicity.

Chapter 2

Goals

Goals can be specified as

1. to describe the principle of the fluxgate magnetometer with relevant physical and engineering background,
2. to give an overview of successful space-born instruments and modern trends in the field of fluxgate magnetometers dedicated to space research,
3. to design, construct and calibrate a fluxgate magnetometer capable of terrestrial measurement of variations of Earth's magnetic field.

Chapter 3

Physical background

3.1 Magnetic field

Magnetic field $\mathbf{B}(\mathbf{r})$ is induced by a charge q moving with velocity $\mathbf{v}$:

$$\mathbf{B}(\mathbf{r}) = \frac{\mu_0}{4\pi}\frac{q}{r^3}(\mathbf{v} \times \mathbf{r}), \tag{3.1}$$

where $\mathbf{r}$ is a vector pointing from the charge to a point of interest. This field acts on moving test charge q_T with velocity $\mathbf{u}$ by magnetic force

$$\mathbf{F} = q_T(\mathbf{u} \times \mathbf{B}). \tag{3.2}$$

For magnetic field induced by current I along path l we reformulate the formula (3.1) to well known Biot-Savart law

$$\mathbf{B}(\mathbf{r}) = \frac{\mu_0}{4\pi} I \int_l \frac{\mathrm{d}\mathbf{l} \times \mathbf{R}}{R^3}, \tag{3.3}$$

where $\mathbf{R} = \mathbf{r} - \mathbf{l}$. Expressing the divergence and the curl of the formula (3.1) we can write laws of magnetism in form

$$\nabla \cdot \mathbf{B} = 0, \tag{3.4}$$

$$\nabla \times \mathbf{B} = \mu_0 \mathbf{j}. \tag{3.5}$$

$\mathbf{j}$ stands for the overall current density including free currents, bound currents, which are results of electromagnetic properties of matter, and the Maxwell displacement current $\epsilon_0 \partial\mathbf{E}/\partial t$. The variable magnetic field generates an electric field given by Faraday law of induction

$$\nabla \times \mathbf{E} = -\frac{\partial \mathbf{B}}{\partial t}. \tag{3.6}$$

We define the inductance L for a current loop, which induces an overall magnetic flux $\Phi = \int_S \mathbf{B} \cdot \mathbf{S}$ by a current I

$$\Phi = LI \tag{3.7}$$

For a system of current loops $1, ..., k$ we define the inductance matrix L_{ij} to express a coupling between loops. The flux through the i-th loop is obtained as a sum of fluxes generated by currents in our system

$$\Phi_i = \sum_{j=1}^{k} L_{ij} I_j. \tag{3.8}$$

L_{ij} are for $i = j$ called self inductances and for $i \neq j$ mutual inductances. Taking the derivative of (3.8) and the induction law (3.6), we obtain dynamic definition of inductance, useful for circuit analysis,

$$U_i = -\sum_{j=1}^{k} L_{ij} \frac{\mathrm{d}I_j}{\mathrm{d}t}. \tag{3.9}$$

More detailed analysis is given in the publication [17].

3.2 Magnetic materials

Magnetic properties of matter result from both existing and induced bound currents inside material bodies. This fact can be described by introducing the magnetizing field $\mathbf{H}(\mathbf{r})$ (generated by external currents $\mathbf{j}_{ext}$) and the magnetization field $\mathbf{M}(\mathbf{r})$ (generated by bound currents $\mathbf{j}_b$).

$$\nabla \times \mathbf{H} = \mathbf{j}_{ext}, \quad \nabla \times \mathbf{M} = \mathbf{j}_b. \tag{3.10}$$

If we neglect the Maxwell displacement current, we can write laws of magnetism as

$$\nabla \times \mathbf{H} = \mathbf{j}_{ext}, \quad \nabla \cdot \mathbf{B} = 0, \quad \mathbf{B} = \mu_0(\mathbf{H} + \mathbf{M}). \tag{3.11}$$

This simplifies magnetic engineering by separating an external field, which can have simple description, and a matter response, which is described by a material function $\mathbf{M}$. The magnetization $\mathbf{M}$ is usually a function of the magnetizing field $\mathbf{H}$ and is useful to introduce the relative permeability μ_r by relation

$$\mathbf{B} = \mu_0 \mu_r \mathbf{H} \tag{3.12}$$

and the differential permeability μ_d by

$$\mathrm{d}\mathbf{B} = \mu_0 \mu_d \mathrm{d}\mathbf{H}. \tag{3.13}$$

Material with weak magnetic interaction has $\mu_r \approx \mu_d \approx 1$.

Ferromagnetism is caused by presence of magnetic domains. Ferromagnetic bodies react on applied magnetizing field by its amplification with hysteresis and they exhibit saturation magnetization. Dependence $\mathbf{M}(\mathbf{H})$ is linear for zero initial magnetization and small applied field. Initial permeability μ_d ranges from 10^2 up to 10^5. Then differential permeability continuously drops approaching 1 in full saturation.

If we remove the magnetizing field, some remanent magnetic field B_R will remain and we need to apply a coercive magnetizing field H_C in opposite direction to remove it entirely. Example of the ferromagnetic magnetization curve is in figure 3.1. More detailed overview can be found in the publication [17].

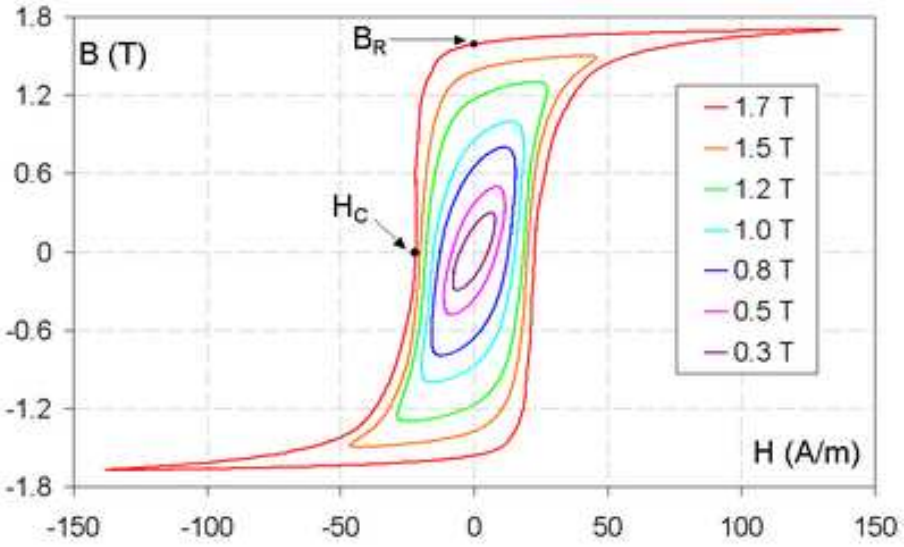

Figure 3.1: Common steel magnetization curves, credit: Wikipedia[18]

3.3 Transformer

We will use introduced theory to explain principle of a transformer. Our system consists of two windings on a cylindrical core. One winding is called the primary, has N_1 turns and is connected to a resistor R_1 and a voltage source $U_1(t)$ in series. Secondary winding with N_2 turns is connected to a resistor R_2 with a voltmeter in parallel. The problem is sketched in figure 3.2.

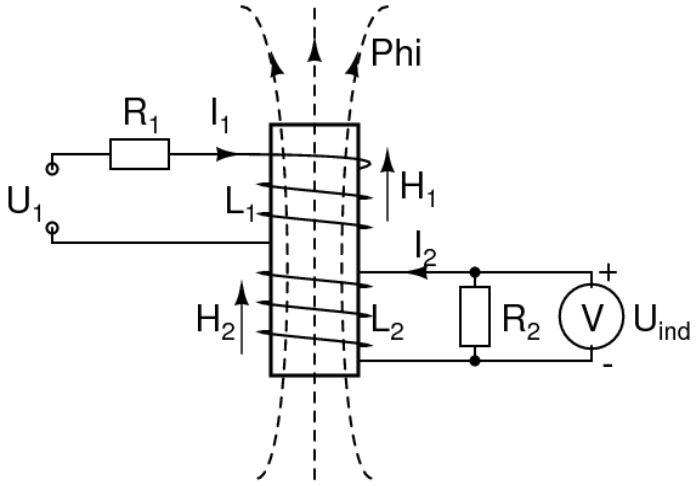

Figure 3.2: Transformer analysis

We can describe both circuits

$$U_1(t) - R_1 I_1 - L_1 \frac{\mathrm{d}I_1}{\mathrm{d}t} - M \frac{\mathrm{d}I_2}{\mathrm{d}t} = 0, \tag{3.14}$$

$$- L_2 \frac{\mathrm{d}I_2}{\mathrm{d}t} - M \frac{\mathrm{d}I_1}{\mathrm{d}t} - R_2 I_2 = 0, \tag{3.15}$$

where L_1 and L_2 are self inductances and M is a mutual inductance.

For long solenoids with volumes V and no flux leakage, we can approximate [17]

$$L_i = \mu_r \mu_0 N_i^2 V, \quad M = \mu_r \mu_0 N_1 N_2 V. \tag{3.16}$$

Problem is transformed into a set of first order ordinary differential equations and can be solved numerically.

If we assume $R_2 \to +\infty$ (open circuit), we can set the second current zero and keep constant the product $U_{ind}(t) = -R_2 I_2$

$$U_1(t) - R_1 I_1 - L_1 \frac{\mathrm{d}I_1}{\mathrm{d}t} = 0, \tag{3.17}$$

$$M \frac{\mathrm{d}I_1}{\mathrm{d}t} = U_{ind}(t). \tag{3.18}$$

With solution

$$U_{ind}(t) = \frac{M}{L_1}(U_1(t) - R_1 I_1). \tag{3.19}$$

Assuming $R_1 = 0$ and idealized inductances (2.15), we obtain well-known formula for transformer with open secondary winding

$$U_{ind}(t) = \frac{N_2}{N_1} U_1(t). \tag{3.20}$$

We assumed the full flux through both windings, but real transformers have some flux leakage. This is the reason for high permeable cores keeping the most flux in their volume and thus lowering a transfer loss. Saturation limits maximal power, which the transformer is capable to efficiently transfer. Those and other aspects are analyzed in the publication [17].

Chapter 4

Principle and basics of fluxgate magnetometers

4.1 Non-linear transformer

The fluxgate magnetometer is based on transformer effect with nonlinear permeability $\mu(\mathbf{H})$ of the core. [15] We will analyze the preceding configuration with the core made by idealized anisotropic material with linear and saturated regions as drawn in figure 4.1.

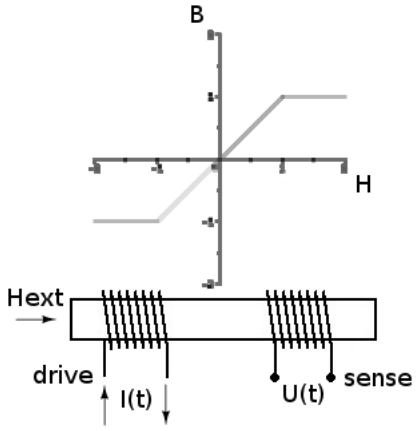

Figure 4.1: Transformer analogy

Induced voltage in the sense winding is proportional to derivative of the flux Φ through the core in longitudinal direction

$$U(t) = -N_2 \frac{\mathrm{d}\Phi}{\mathrm{d}t} \approx -N_2 S \frac{\partial B}{\partial t} = -\mu_0 N_2 S \frac{\mathrm{d}}{\mathrm{d}t}(\mu_r(H)H). \tag{4.1}$$

The magnetizing field component H is a sum of the drive (excitation) winding magnetization H_D and the external magnetic field component H_{ext}

$$H = H_D[I(t)] + H_{ext}. \tag{4.2}$$

Assuming H_{ext} constant, we can rewrite the mechanism to

$$U(t) \approx -\mu_0 N_2 S \frac{\mathrm{d}H_D}{\mathrm{d}I}\frac{\mathrm{d}I}{\mathrm{d}t}\left(\left.\frac{\mathrm{d}\mu_r}{\mathrm{d}H}\right|_H H + \mu_r|_H\right). \tag{4.3}$$

The dependence on the external field is slightly hidden in permeability and its derivative parameters.

If we drive the primary winding with a sinusoidal current signal into saturation, we obtain derivative of induced magnetic flux Φ. Undisturbed output is an odd function relative to every zero-crossing point. It implies zero second harmonic signal in the output.

An external magnetizing field in longitudinal direction disturbs this symmetry because it shifts the core into the saturation earlier, when we drive it to the same direction as the external field, and later for the opposite direction. This brings a second harmonic signal into the output. It is possible to filter out the second harmonic, obtain its phase and rectify it to obtain a steady value proportional to a magnitude of the external field, but the presence of large original signal complicates the extraction of measured signal.

4.2 Differential measurement

Vacquier's design consists of two symmetrical anti-parallel drive windings and common sense winding. [15] See figure 4.2.

Without an external field, the flux induced in the first drive winding has an opposite direction to that induced by the second drive winding with equal magnitudes for both. Consequently, there is zero signal in the output. Let's drive our cores periodically deep into saturation. An external magnetizing field H_{ext} shifts one core into saturation earlier and other one later than in undisturbed case. This results in a signal in the sense winding sketched in figure 4.2

Induced voltage in the sense winding with N_S turns is proportional to derivative of both fluxes $\Phi = \Phi_1 + \Phi_2$

$$U(t) = -N_S\frac{\mathrm{d}\Phi}{\mathrm{d}t} \approx -N_S S\frac{\mathrm{d}B}{\mathrm{d}t} = -\mu_0 N_S S\frac{\mathrm{d}}{\mathrm{d}t}(\mu_r|_{H_1}H_1 + \mu_r|_{H_2}H_2), \tag{4.4}$$

where

$$H_1 = H_D + H_{ext}, \quad H_2 = -H_D + H_{ext}, \tag{4.5}$$

S is sum of cross-sections of both cores and H_D is the magnetizing field induced by a drive signal.

Expanding the formula (4.4) and assuming H_{ext} constant, we obtain

$$U(t) \approx -\mu_0 N_S S\frac{\mathrm{d}H_D}{\mathrm{d}I}\frac{\mathrm{d}I}{\mathrm{d}t}\left(\frac{\mathrm{d}\mu_r|_{H_1}}{\mathrm{d}H}H_1 + \frac{\mathrm{d}\mu_r|_{H_2}}{\mathrm{d}H}H_2 + \mu_r|_{H_1} - \mu_r|_{H_2}\right), \tag{4.6}$$

Let's assume $\mu_r(H) = \mu_r(-H)$ (isotropy of the core) and $|H_{ext}| \ll |H_D|$ (this assumption is valid, when overall flux is not zero). Then we can approximate

$$\mu_r|_{H_1} \approx \mu_r|_{H_D} + \left.\frac{\mathrm{d}\mu_r}{\mathrm{d}H}\right|_{H_D} H_{ext}, \quad \mu_r|_{H_2} \approx \mu_r|_{H_D} - \left.\frac{\mathrm{d}\mu_r}{\mathrm{d}H}\right|_{H_D} H_{ext}, \tag{4.7}$$

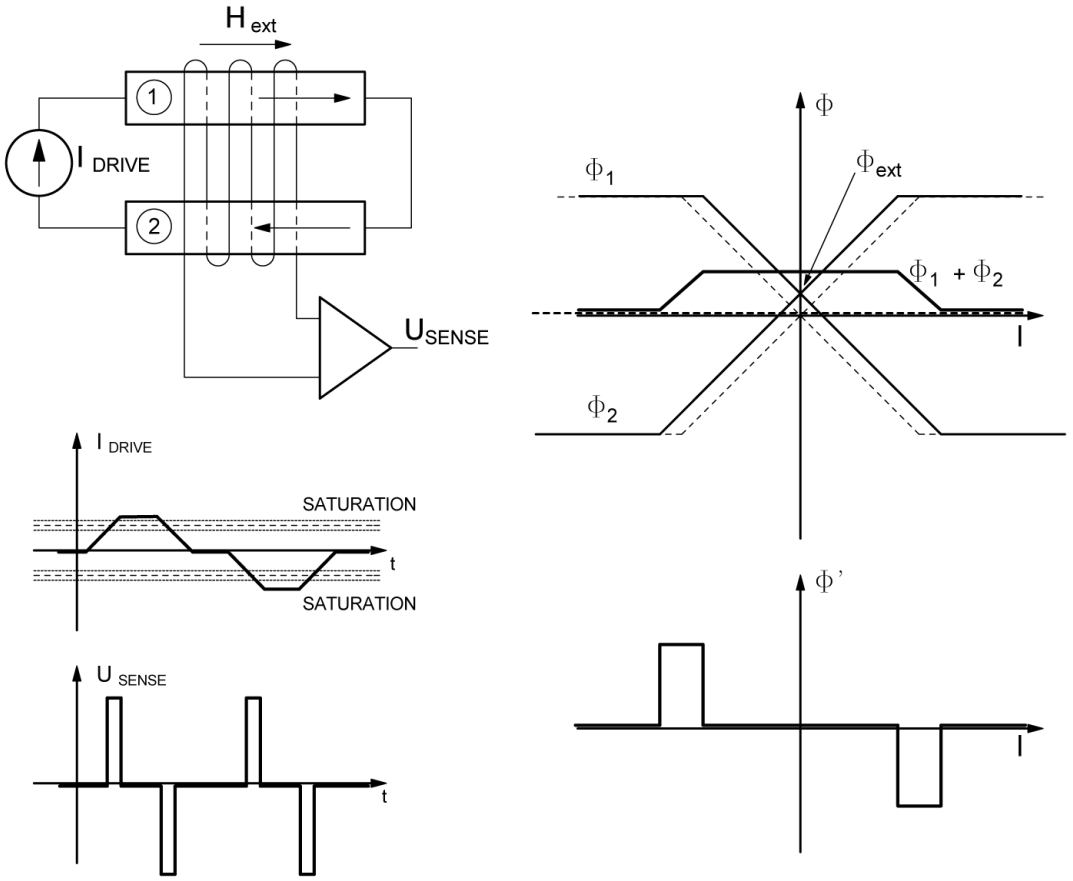

Figure 4.2: Clockwise: Vacquier's configuration scheme, $\Phi(I)$ diagram undisturbed (dashed) and disturbed (full), disturbed $\frac{\mathrm{d}\Phi(I)}{\mathrm{d}I}$ diagram, Example disturbed waveform

$$\frac{\mathrm{d}\mu_r|_{H_1}}{\mathrm{d}H} = \frac{\mathrm{d}\mu_r}{\mathrm{d}H}\bigg|_{H_1} H_1 \approx \left(\frac{\mathrm{d}\mu_r}{\mathrm{d}H}\bigg|_{H_D} + \frac{\mathrm{d}^2\mu_r}{\mathrm{d}H^2}\bigg|_{H_D} H_{ext}\right)(H_D + H_{ext}) \tag{4.8}$$

and

$$\frac{\mathrm{d}\mu_r|_{H_2}}{\mathrm{d}H} = -\frac{\mathrm{d}\mu_r}{\mathrm{d}H}\bigg|_{H_2} H_2 \approx \left(\frac{\mathrm{d}\mu_r}{\mathrm{d}H}\bigg|_{H_D} - \frac{\mathrm{d}^2\mu_r}{\mathrm{d}H^2}\bigg|_{H_D} H_{ext}\right)(-H_D + H_{ext}). \tag{4.9}$$

Notice $H_D \approx N_D I$, where N_D is number of turns in each drive winding. Neglecting higher orders gives us

$$U(t) \approx -\mu_0 N_S N_D S \frac{\mathrm{d}I}{\mathrm{d}t} H_{ext}\left(4\frac{\mathrm{d}\mu_r}{\mathrm{d}H}\bigg|_{H_D} + 2\frac{\mathrm{d}^2\mu_r}{\mathrm{d}H^2}\bigg|_{H_D} H_D\right). \tag{4.10}$$

First term in parentheses is our signal. For our idealized material and symmetrical square wave, it is phase synchronized with driving signal and occurs with twice-frequency of the drive. Second term is more problematical, but simple considerations for our idealized material shows it is a quick phenomenon, which will disappear after integration. Further examination is needed for real materials.

To improve sensitivity, we can add more turns to both windings, increase the sensor cross-section, use faster transition driving signal and high-permeable core with sharp transition into saturation. It is important to drive the core deep into saturation.

The output signal is present when permeability is changing (linear/saturated transition) and is proportional to the asymmetry introduced by the external field. The sign is determined by a current direction, an external field orientation and by the core transition in/out of the saturation.

One way of output processing is the second harmonic demodulation. We integrate the signal only in moments of positive polarity of the output signal for chosen external field orientation. Measuring electronics needs to be phase synchronized with driving electronics. This principle is drawn in figure 4.3.

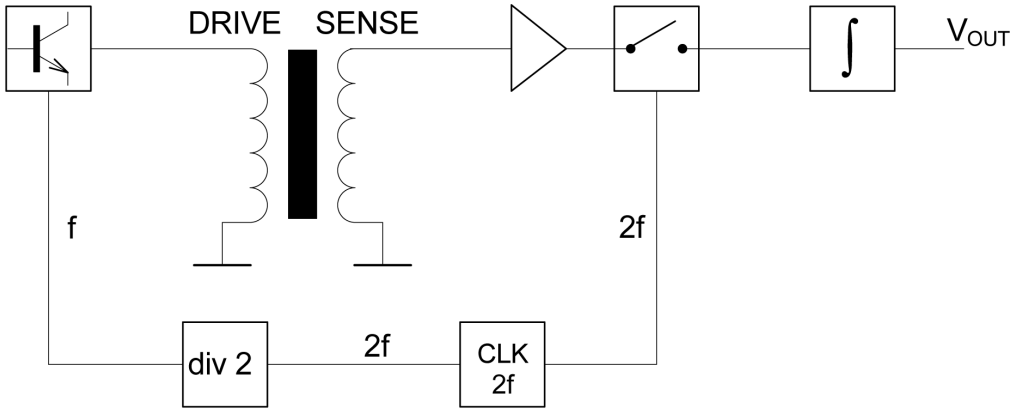

Figure 4.3: Principle of second harmonic demodulation fluxgate magnetometer

4.3 Feedback measurement

To increase the range and the linearity we can add the Helmholtz coils pair as a compensation winding. The signal proportional to the field measured by the fluxgate is amplified and fed to Helmholtz coils against the external field. This forms a negative feedback compensating an external field. It is simple to measure the compensating current, which is directly proportional to the external field. Two extra windings can be spared by using DC isolated measurement path and feeding the compensation directly to the sense winding. [15] Such system is sketched in figure 4.4.

4.4 Materials for fluxgate sensors

From preceding facts we can state some requirements for core materials. High permeable core magnetizes quickly and for low magnetizing field is saturated. This means that transition occurs for lower ratio H_{ext}/H_D. Also it lowers required magnetization current and thus power consumption of drive electronics.

Low coercive force and low remanence leads to separation of transitions of different polarities.

Other required properties are low Barkhausen noise (caused by discrete nature of the process), low magnetostriction and low internal stresses to decrease sensor noise.

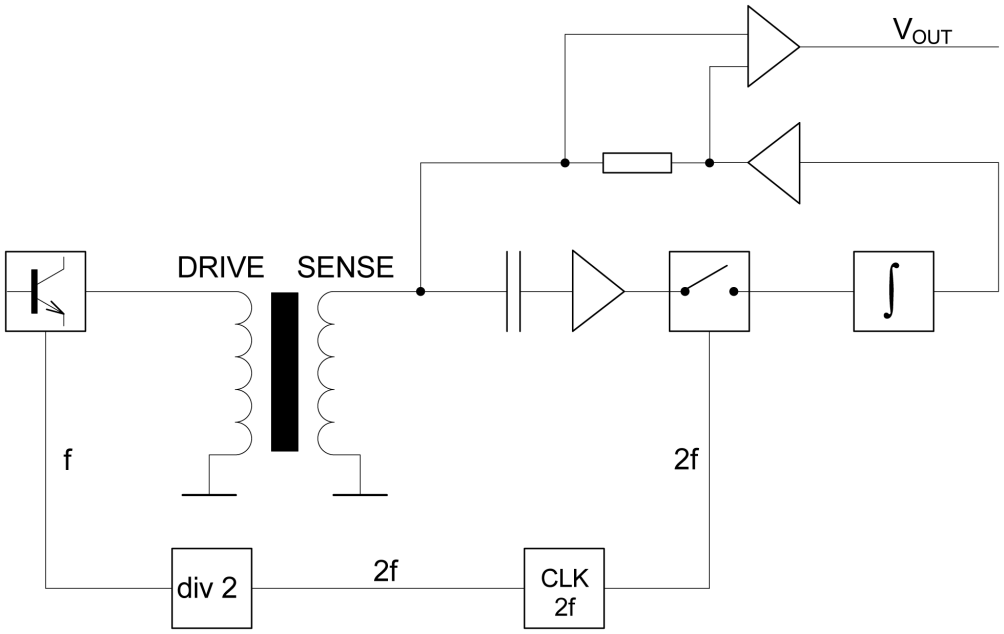

Figure 4.4: Second harmonic demodulation fluxgate magnetometer with feedback measurement

Also low structural imperfections, uniform properties, low deformations and low mechanical stress decrease sensor offset and improve stability.[15]

4.5 Sensor designs and multi-axial measurement

There are other uni-axial designs exploiting similar principles: racetrack, ring core or Förster's anti-parallel configuration. See figure 4.5.

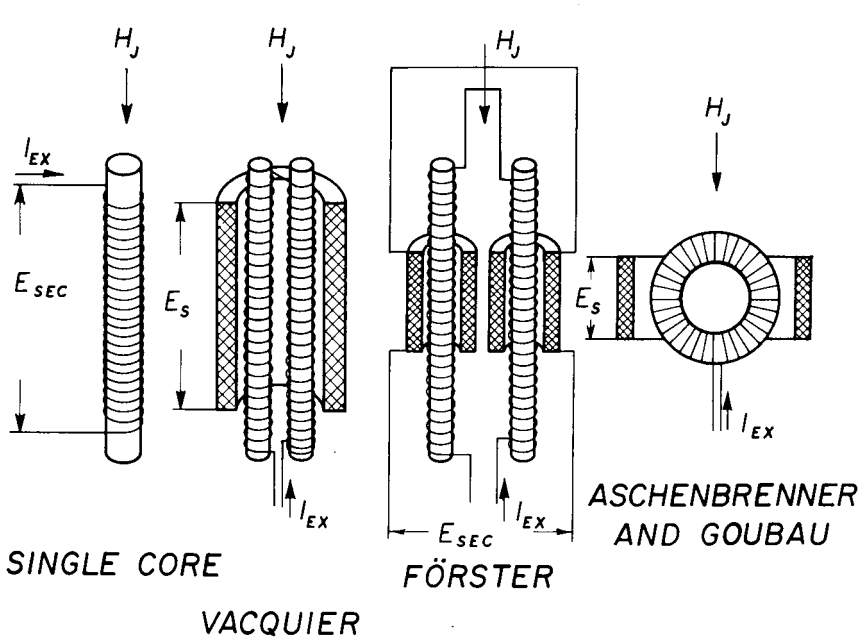

Figure 4.5: Different uni-axial sensors, credit: Fritz Primdahl [14]

Bi-axial magnetometer can be implemented by the ring core design with two orthogonal sense windings. Tri-axial measurement is more complicated. Multiple ring cores in an orthogonal layout are used. Figure 4.6 shows example of a successful design.

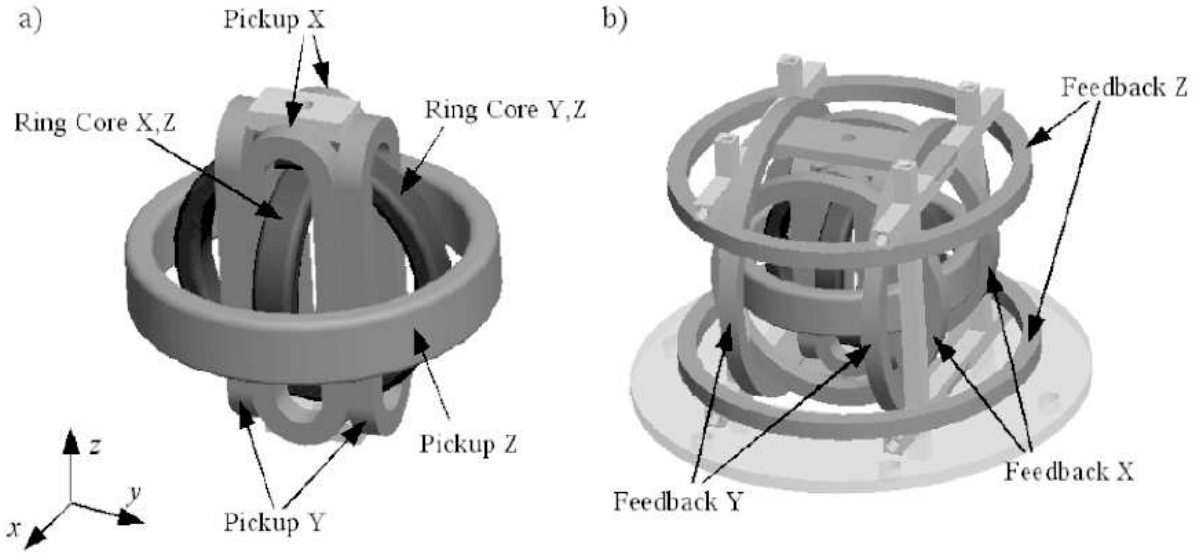

Figure 4.6: THEMIS sensor, credit: Auster et al. [1]

Advanced fluxgate magnetometer design called compact spherical coil (CSC) is an extension of this approach. It consists of the tri-axial magnetometer inside a spherical system of compensation (feedback) coils. [12] Photography is in figure 4.7.

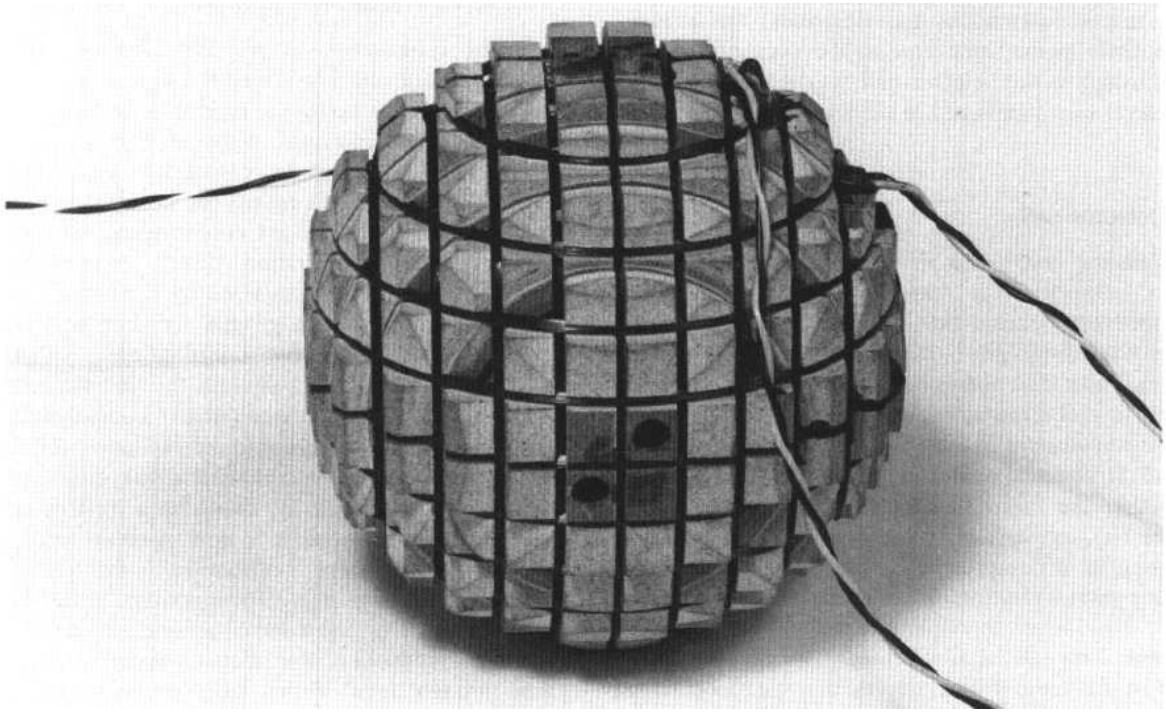

Figure 4.7: Ørsted Compact spherical coil, credit: Nielsen et al.[12]

Chapter 5

Successful instruments, proposed designs and trends

5.1 Ørsted magnetometers

The Danish satellite Ørsted is dedicated to precise mapping of Earth's magnetic field and was launched in 1997. It orbits our planet in height ranging from 600 to 850 km. The scientific payload consists of star camera, particle detector and vector and scalar magnetometers. These instruments are placed on a deployable boom eight meters long to avoid interfering with on-board electronics. The Ørsted measurement revealed accelerating shift of North Earth's magnetic pole. Earth's magnetic field reversal is now subject of intensive research and can have a significant effect on terrestrial life. [6]

The Overhauser scalar magnetometer is used for scalar calibration of the vector magnetometer. Advanced vector magnetometer is of the CSC fluxgate type. Block diagram of one channel of the tri-axial fluxgate magnetometer is in figure 5.1. Excitation electronics is implemented as full MOSFET H-bridge and utilizes single +5 V supply. The excitation circuit is on figure 5.2.

The sense electronics is implemented as an analog switched integrator. The measurement is feedback based. Figure 5.3 shows the sense electronics.

The output is sampled by 16-bit ADC which limits the resolution to 0.5 nT. Range of the fluxgate magnetometer is $\pm 65\,\mu$T. Power consumption is about 1 W. This device shows high reliability and is still operating from 1999, 6x times exceeding required operating life. [12]

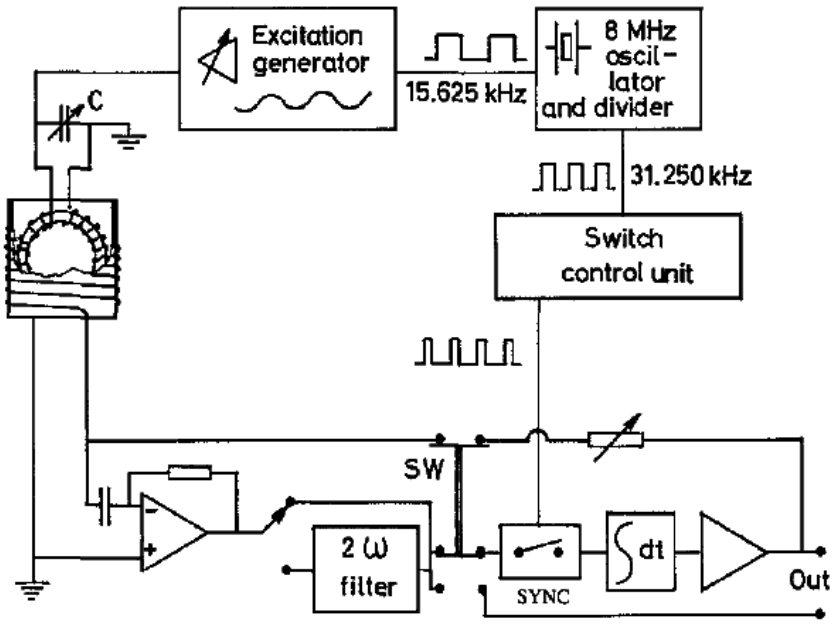

Figure 5.1: One channel of Ørsted fluxgate magnetometer electronics, credit: Nielsen et al.[12]

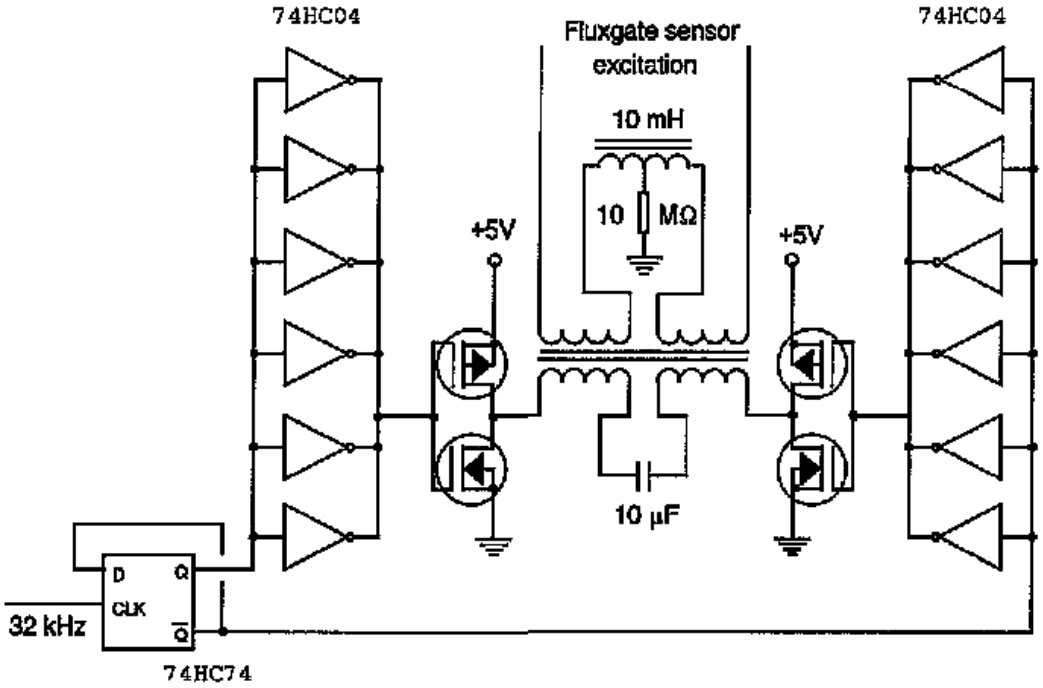

Figure 5.2: Ørsted drive (excitation) electronics, credit: Nielsen et al.[12]

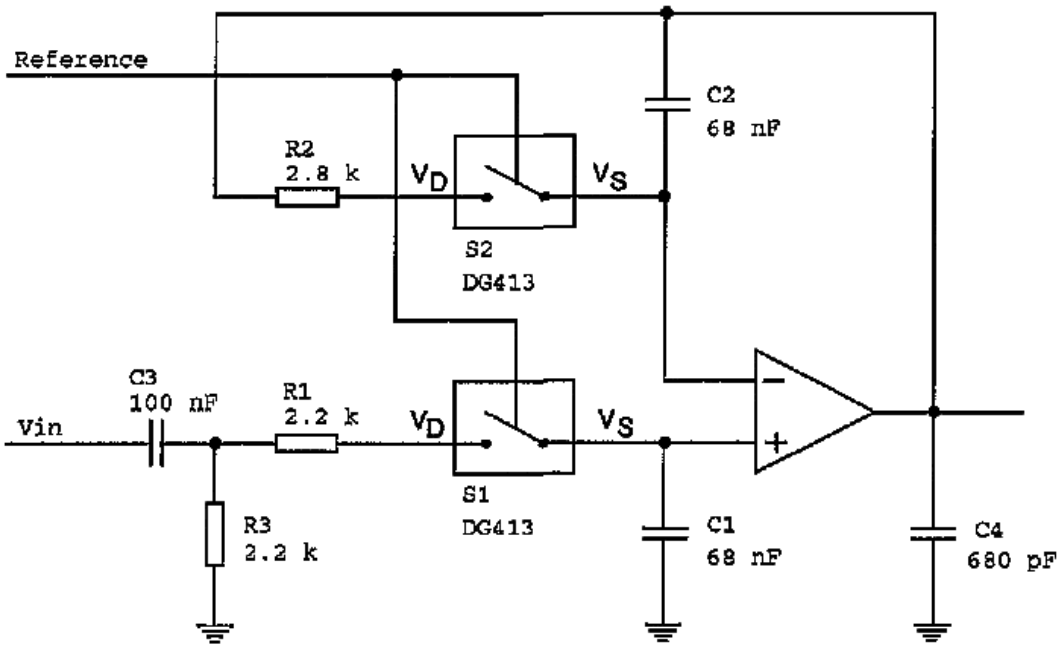

Figure 5.3: Ørsted sense electronics, credit: Nielsen et al.[12]

5.2 THEMIS magnetometers

THEMIS stands for Time History of Events and Macroscale Interactions during Substorms. This NASA mission consists of five satellites on different orbits inside the magnetosphere and around the Moon. It is dedicated to study overall evolution of space weather. The whole system is designed to measure conditions in the solar wind, the magnetosheath, the magnetotail and in other parts of the magnetosphere in between $1R_E$ (Earth radii) and $30R_E$ in various configurations at the same time.

Probes frequently cross radiation belts and all instrumentation works in broad range of conditions. Very advanced electronic design digitalizes most processes on a field programmable array (FPGA). Figure 5.4 shows a block diagram of the system. Design of the fluxgate sensor is based on three concentric orthogonal ring cores with different diameters. Sense windings and feedback windings are separated. See figure 4.6. Range of fluxgate magnetometer is $\pm 25\,\mu$T and resolution: 3 pT. Proven stability is 0.5 nT per half a year. [1]

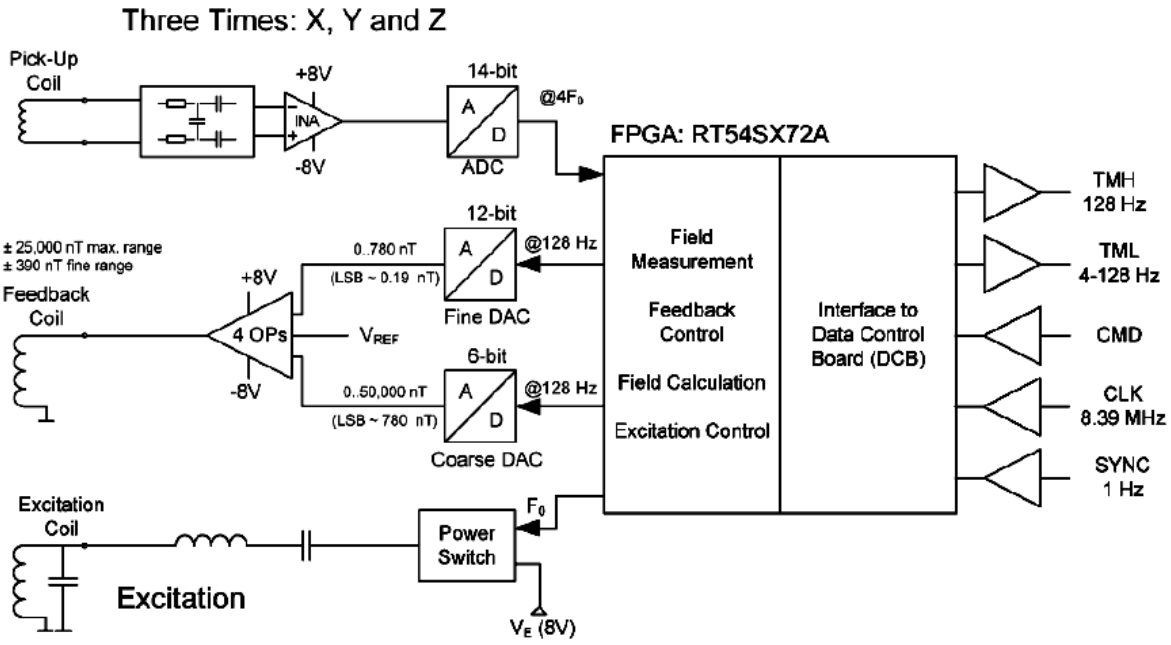

Figure 5.4: THEMIS magnetometer electronics, credit: Auster et al. [1]

5.3 Other designs and trends

Review of some other ongoing and future missions shows general shift from analog devices to digital instrumentation. Large FPGA and fast ADC and DAC converters implement digital signal processing, drive and compensation control, sensors and electronics temperature control, output data compression, power management, data interfacing to the spacecraft and other tasks. Mechanisms for on-flight calibration were developed. [8][5]

There is a general requirement for reduction of power consumption, weight and dimensions.

Chapter 6

Design and prototyping

6.1 Approach

Chosen electronic design exploits digital control of the excitation electronics together with digital output signal processing. This approach is a compromise between an analog 2nd harmonic demodulation system and modern digital design implemented on FPGA, which I am unfortunately not experienced with.

This approach will require digitally interfaced drive electronics, sense amplifier, conditioning circuit and fast analog-digital converter (further only ADC). Simple communication interfaces, as is serial peripheral interface (further only SPI), are preferred. Block diagram of this general idea is sketched in figure 6.1.

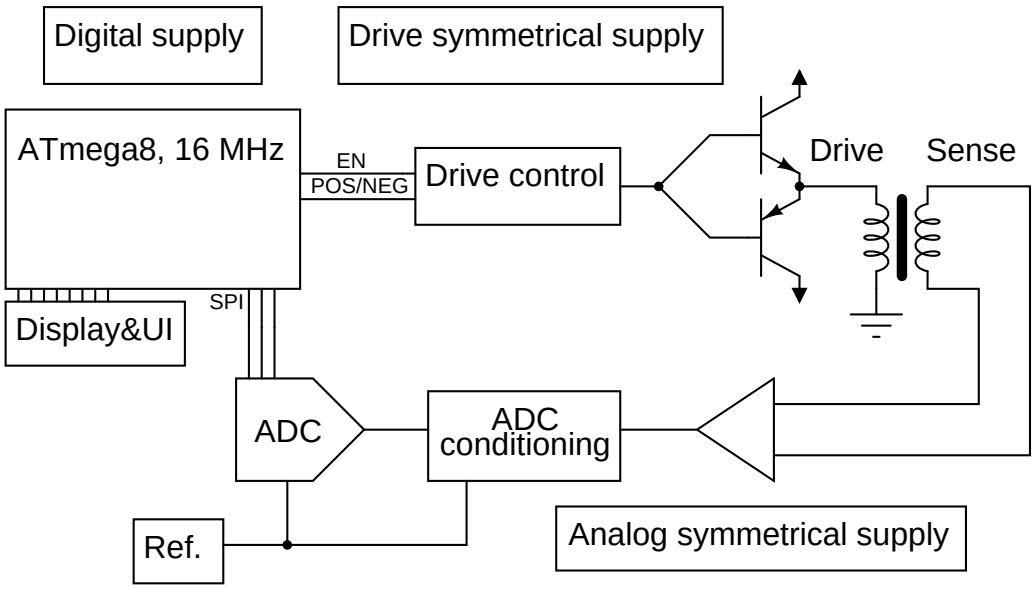

Figure 6.1: General idea of digitally controlled 2nd harmonic demodulation fluxgate magnetometer

6.2 Prototyping

I used to develop electronic devices by the following procedure. First, all required abilities and properties of device are written out and a block diagram is sketched. Then electronics is divided into subsystems with defined tasks. Then again, all required functions are written out for every subsystem with input and output specifications.

Schematics is designed by hand and the proposed circuit is simulated. I use simple open source circuit simulator by Paul Falstad [7]. Component values are adjusted to improve performance and to minimize currents in the system. Then the circuit is tested on a breadboard and soldered on a prototyping board. SMD components are preferred because of compactness of the resulting device.

Useful tool is open source electronic construction kit *MLAB*. It provides reliable and universal prototyping platform. MLAB kit consists of a base board with 3 mm holes aligned to 400 mil (0.4 inch, 10.16 mm) grid and set of various modules as power supplies, basic microcontroller circuits of different architectures (AVR, PIC and ARM), their programmers, communication devices, ADC and DAC modules, sensors, human interface devices and many others. See MLAB homepage for exhausting list and description of modules [11].

6.3 Control unit and communication interface

I chose 8-bit RISC microcontroller (further only μC) architecture *Atmel AVR* which I am experienced with. It executes most instructions in single cycle including multiplication and there is a rich on-chip peripheral selection. It is simple to develop a firmware in *C programming language*. There is a complete open source development toolchain consisting of *avr-gcc* compiler, *avr-libc* library and *avr-binutils* tools. [3] Also there are *uisp* and *avrdude* uploaders compatible with wide range of programming hardware.[13]

ATmega μCs are simple to program directly in application (*ISP* feature, in-system programming), they have sufficient internal program memory and SRAM and μC includes on-chip timers, counters and hardware SPI, I^2C and USART communication devices.

The first stage of development utilized my own *ATmega8* μC prototyping circuit and a simple homemade programmer. It is described in my tutorial [13] including installation of the complete AVR development toolchain in GNU/Linux. In later development stage I moved to MLAB modules *ATMEGA801B*, basic ATmega8 μC circuit, and *ATprogISPUSB02A* USB programmer compatible with AVR *STK500v2* interface. Complete documentation is available on MLAB website [11]. μC is clocked by 16 MHz crystal.

All user interfacing is implemented as a serial communication between the ATmega8 USART (universal synchronous/asynchronous receiver/transmitter) communication device and a personal computer (further only PC). In the earliest stage of development I had been using a simple MAX232 based TTL-RS232 translator and depre-

cated PC serial port with baud rate 115.2 kBd. Current development stage utilizes *USB232R01B* MLAB module. This module is a basic circuit for the *FT232RL* USART-USB translator IC. This device has a native Linux driver translating the communication to a common serial terminal, which appears as a */dev/ttyUSBX* device file (where X stands for 0, 1, 2...). All communication is simplified to reading and writing this device file. FT232RL module allows baud rate up to 1 MBd.

It is important to disable character echoing and terminal control signals for full binary data transfer. This together with baud rate setting can be done on PC side using GNU *stty* utility:

```
stty -F /dev/ttyUSB0 1000000 raw -hupcl
```

See stty manual for details [9]. μC setting is described in firmware section.

μC, communication and programmer modules are supplied from USB +5 V power line.

Fluxgate magnetometer performs requested action after receiving a specified byte. Data exchange is implemented as a binary transfer. The whole operation is described in the last section of this chapter. Block diagram of implemented system is in figure 6.2. Photography of assembled MLAB board is in figure 6.3.

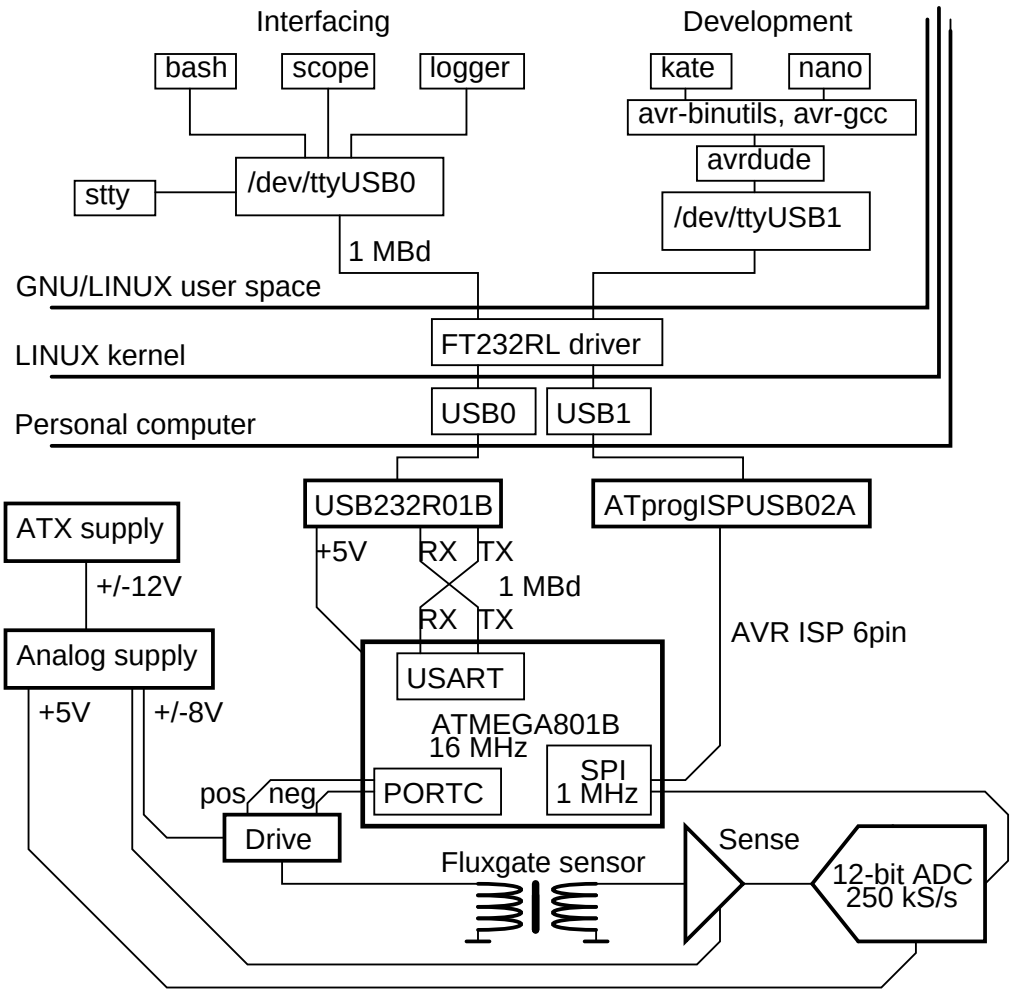

Figure 6.2: System architecture and communication

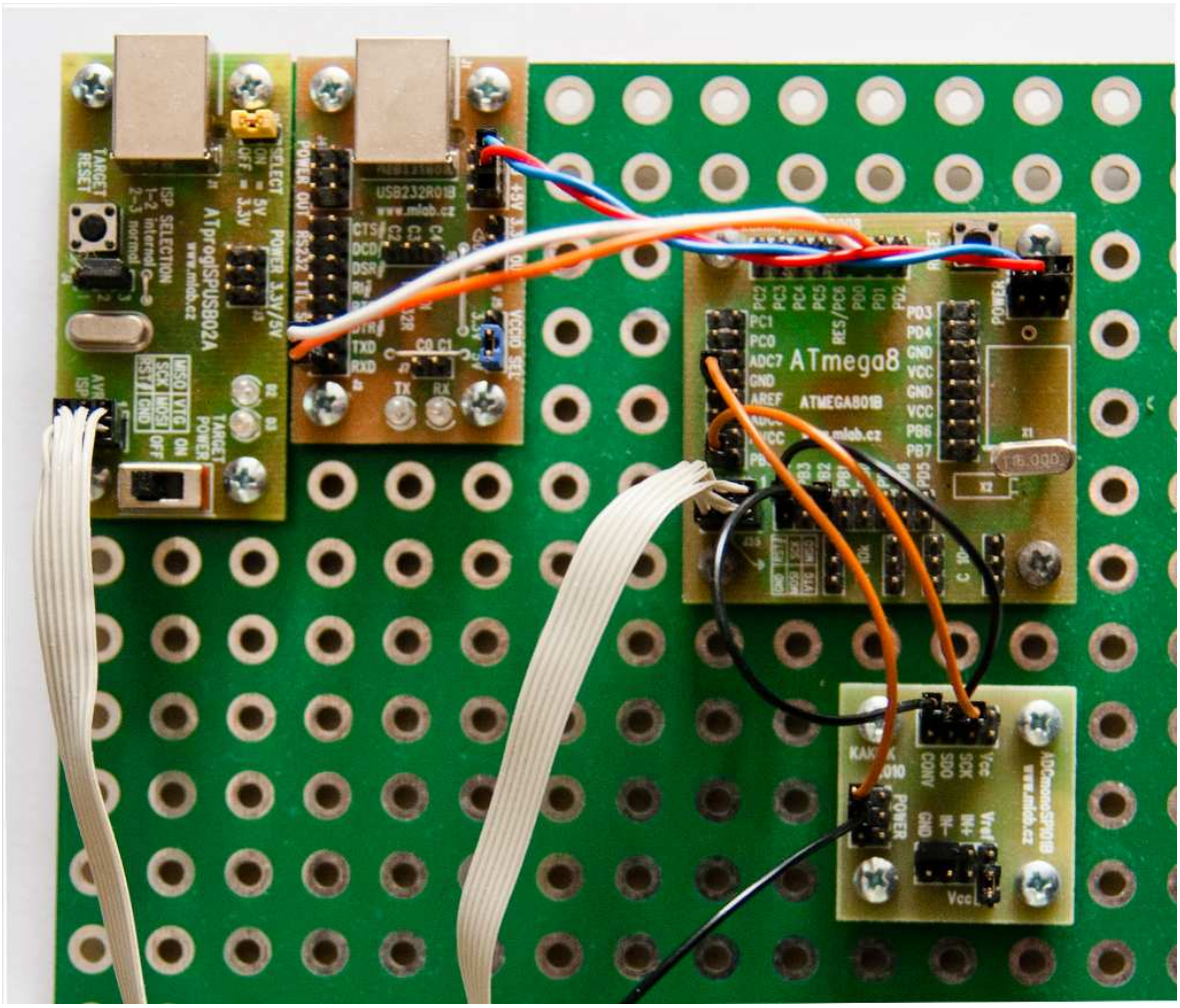

Figure 6.3: Control and communication system with the ADC build from MLAB kit parts

6.4 Drive electronics

I proposed simple optically-triggered bipolar half bridge with a symmetrical supply as an alternative to commonly used H-bridge drive. Advantages are simplification of digital interface, physically smaller electronics and optical isolation from the digital circuit. The drive electronics scheme is in figure 6.4. It is supplied from the drive symmetrical supply based on *LM7808/LM7908* pair.

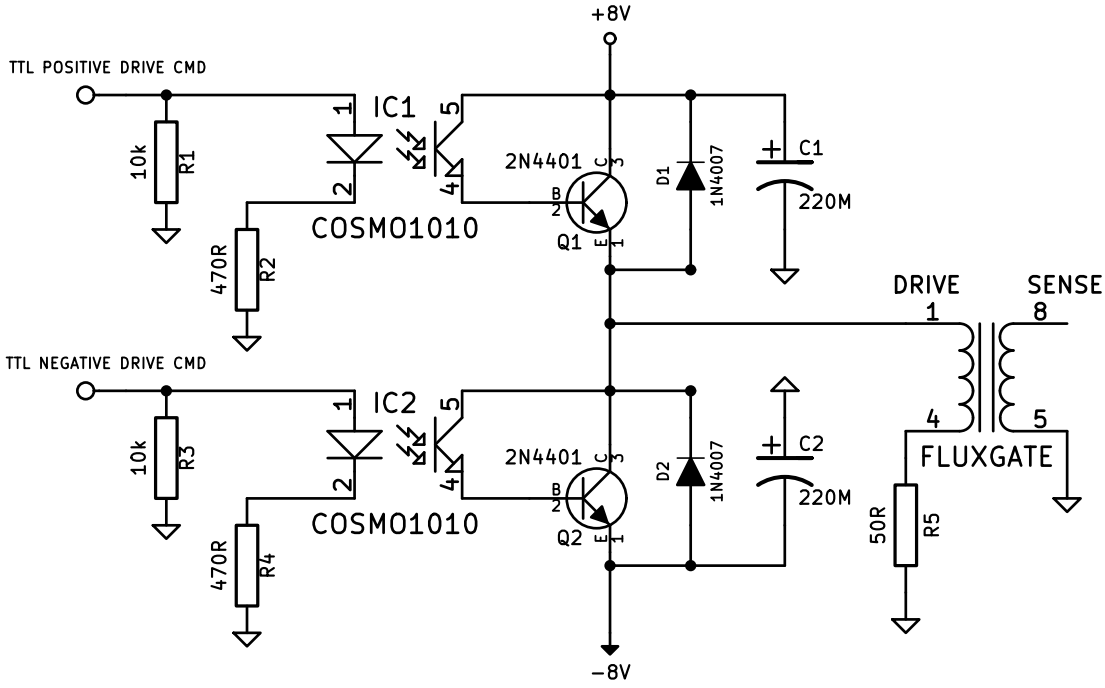

Figure 6.4: Drive electronics

6.5 Sense electronics

The sense electronics consists of a DC blocking passive filter followed by a non-inverting amplifier based on the low noise, low offset *OP07C* bipolar operational amplifier (further only opAmp). Next stage is a summing amplifier. It shifts the signal zero level to 2.5 V because of single-supply ADC operation. Last section before ADC is simple a Zener diode clamp, protecting the ADC input against voltages above 5.1 V and under -1 V.

The gain of amplifier is set to cover ADC range. This analog path is supplied by another LM7808/LM7908 pair.

The ADC *LTC1864* was chosen because of its 16-bit resolution, 250 kS/s sampling rate, serial SPI-compatible output and its availability as *ADCmonoSPI01B* MLAB module. Disadvantage for this application is single supply operation. The ADC is powered by *LM317T* based +5 V supply. The sense scheme is in figure 6.5.

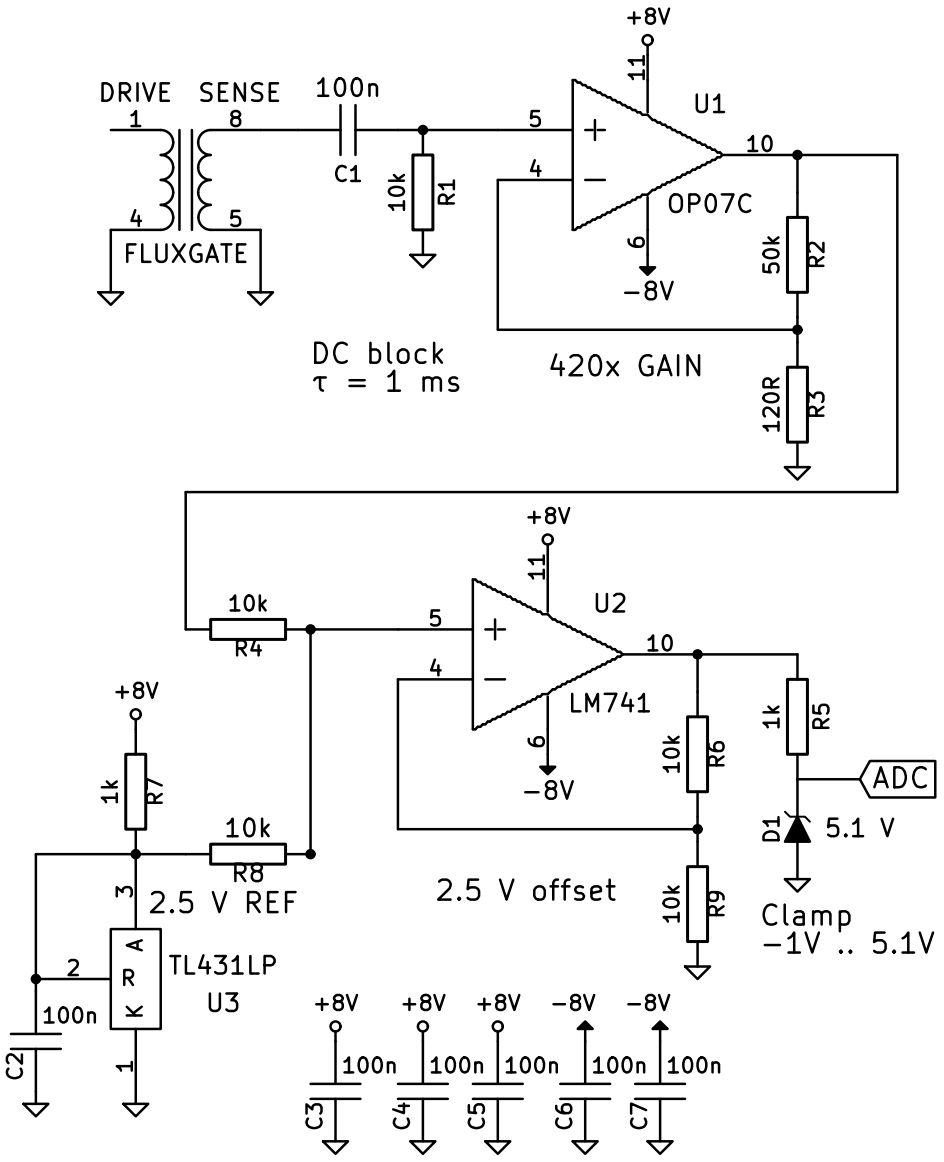

Figure 6.5: Sense electronics

6.6 Sensor

The first sensor was constructed for testing of electronics. It consists of the iron wire 1.5 mm in diameter, 45 cm long. Excitation winding was winded along its full length by approximately 400 turns. Then the wire was bended in its half to form parallel symmetrical pair of long solenoids connected in sharp knee. Then the sense (pick-up) coil was winded over the excitation pair. See photography in figure 6.6. Similar sensor is described in the article [4].

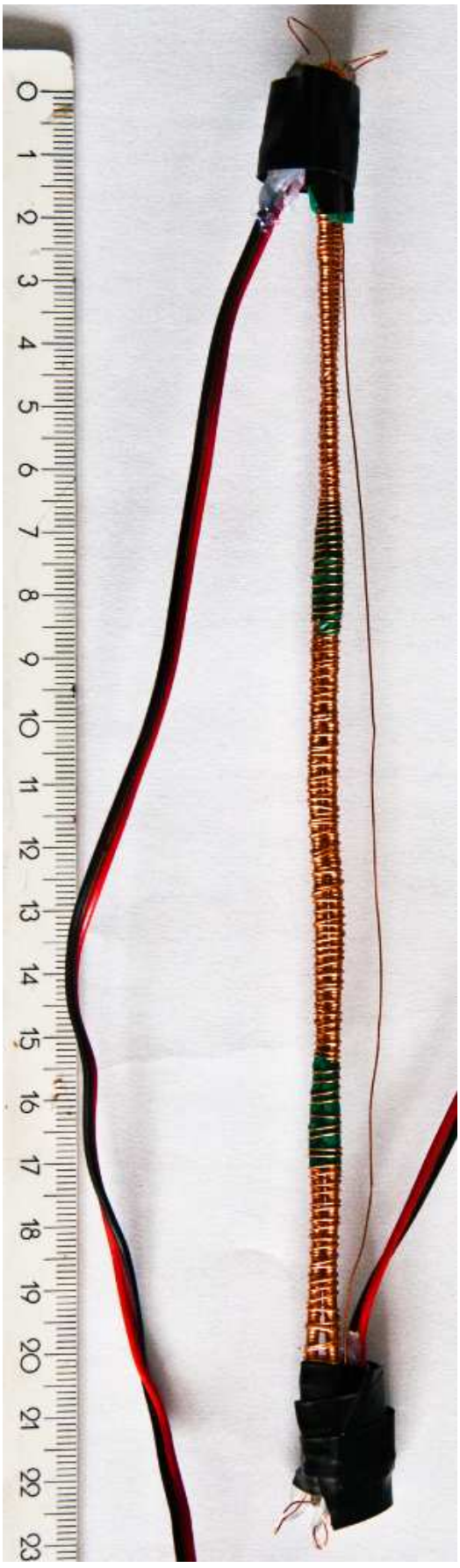

Figure 6.6: My sensor

6.7 Firmware, software and operational procedure

μC is programmed in the C programming language. Its operation can be described by following pseudocode:

```
main() {
  set_pins_directions();
  USART_init(1 MBd, 8 bits, no parity, 1 stop bit,
             asynchronous, USART receive interrupt enable);
  SPI_init(Master, 1 Mhz);
  set_interrupt();

  while (1) {};
}


USART_receive_interrupt_routine() {
  clear_interrupt;

  if (recieved=='a')
    send_waveform();
  else if (recieved=='v')
    send_value();

  set_interrupt();
}


send_waveform() {
  for(j=0;j<32;j++) { // to charge blocking capacitors
    for(i=0;i<128;i++) {
      drive(i);
      _delay_us(5);
    }
  }

  for(i=0;i<128;i++) {
    drive(i);
    data[i]=SPI_get_ADC_value();
    delay_us(4);
  }

  drive_off();
  USART_transmit(data);
}


send_value() {
```

```
  for(j=0;j<32;j++) { // to charge blocking capacitors
    for(i=0;i<128;i++) {
      drive(i);
      _delay_us(5);
    }
  }

  for(i=0;i<128;i++) {
    drive(i);
    if (i<32)  // even harmonic demodulation:
      result = result + SPI_get_ADC_value();
    else if ( (i>=64) && (i<96) )
      result = result - SPI_get_ADC_value();
    delay_us(4);
  }

  drive_off();
  USART_transmit(result);
}


drive(i) {
  if (i<64) {
    negative_drive_pin=0;
    positive_drive_pin=1;
  } else {
    positive_drive_pin=0;
    negative_drive_pin=1;
  }
}


drive_off() {
  positive_drive_pin=0;
  negative_drive_pin=0;
}
```

The actual code is included on the enclosed CD-ROM.

Debugging is possible by simple bash commands (don't forget stty setting described in the communication section)

```
cat /dev/ttyUSB0 &
echo -n a > /dev/ttyUSB0
echo -n v > /dev/ttyUSB0
```

This is simple and powerful tool in combination with output redirecting and utilities as GNU gnuplot, but it shows it is more comfortable to write two graphing PC programs. *Scope* and *logger* are written in C++ using the qT graphical toolkit to direct plotting of measured data. (The qT is for its simplicity, programming paradigm,

documentation and completeness the best graphical API I have ever worked with.)

The *scope* periodically asks by sending 'a' for a measured waveform and plots it. Nothing can be simpler:

```
void Scope::getData() { // Called every 100 ms
  char c='a';
  data=new char[LEN*sizeof(char)];

  FILE *serial=fopen("/dev/ttyUSB0","r+");
  fwrite(&c,sizeof(char),1,serial);
  fread(data,sizeof(char),LEN,serial);
  fclose(serial);

  dataAquired=1;
  update(); // update the screen
}
```

The *logger* acts very similarly. By periodically sending 'v' it plots the evolution of measured value in time. The complete code of both programs is on enclosed CD-ROM.

Chapter 7

Testing

Procedure begins by setting the serial communication on the PC and switching on the analog power supply. We can start the *scope* to see measured waveform before the demodulation. Gain of sense amplifier has to be set to maximize usage of full ADC range. We see reserves on the following screen-shot. Also there is a strong feed-through of the excitation signal. Those effects are investigated in the following chapter.

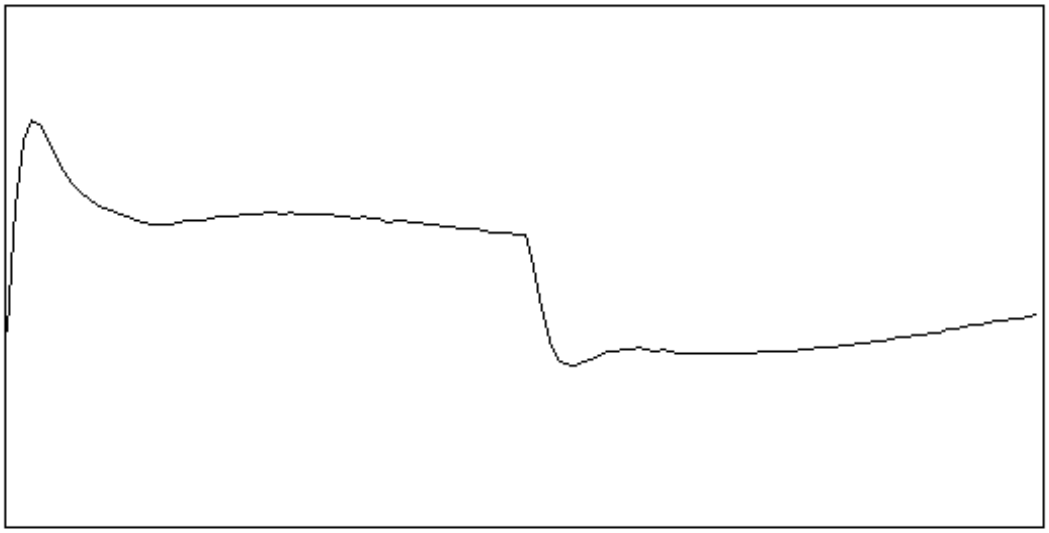

Figure 7.1: Typical waveform plotted by the *scope*

We exit the *scope* and start the *logger*. The sensor sends now an integral value. It can vary in dependence on actual setting of the device everywhere in between $\pm 10^5$. This is the reason for adjustable parameters $shift$ and $divisor$. Graphed y-coordinate is then computed as

$$y = \frac{input + shift}{divisor} \tag{7.1}$$

We see two sliders, bigger for setting the $shift$ (offset) and smaller for the $divisor$. First we set the $shift$ to move the signal level to central horizontal line, than lower

the divisor, than again adjust the offset and so on, until the divisor is set to minimal value 1. Result looks as figure 5.2.

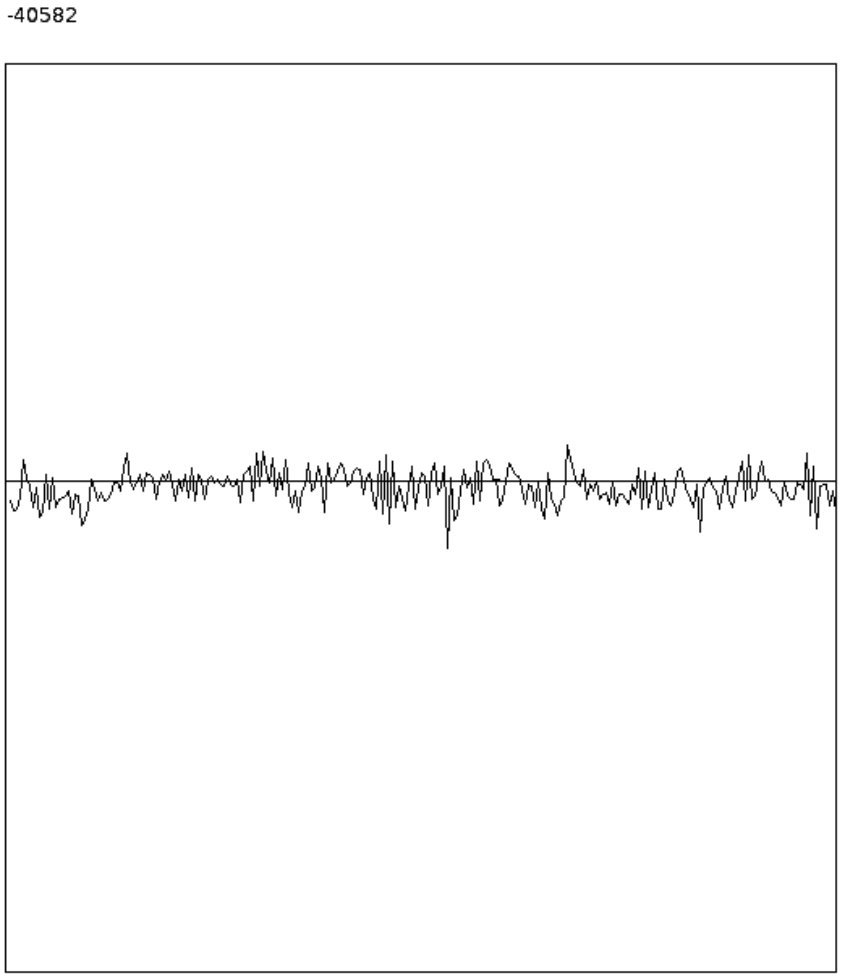

Figure 7.2: Adjusted shift and divisor of *logger*

We can verify the basic function by a common fridge magnet being rotated ca 15 cm from the sensor head. This is a problematical verification because length of our sensor is large in comparison to magnet's size and its characteristic distance of field variation, but we obtained expected result as seen in figure 5.3.

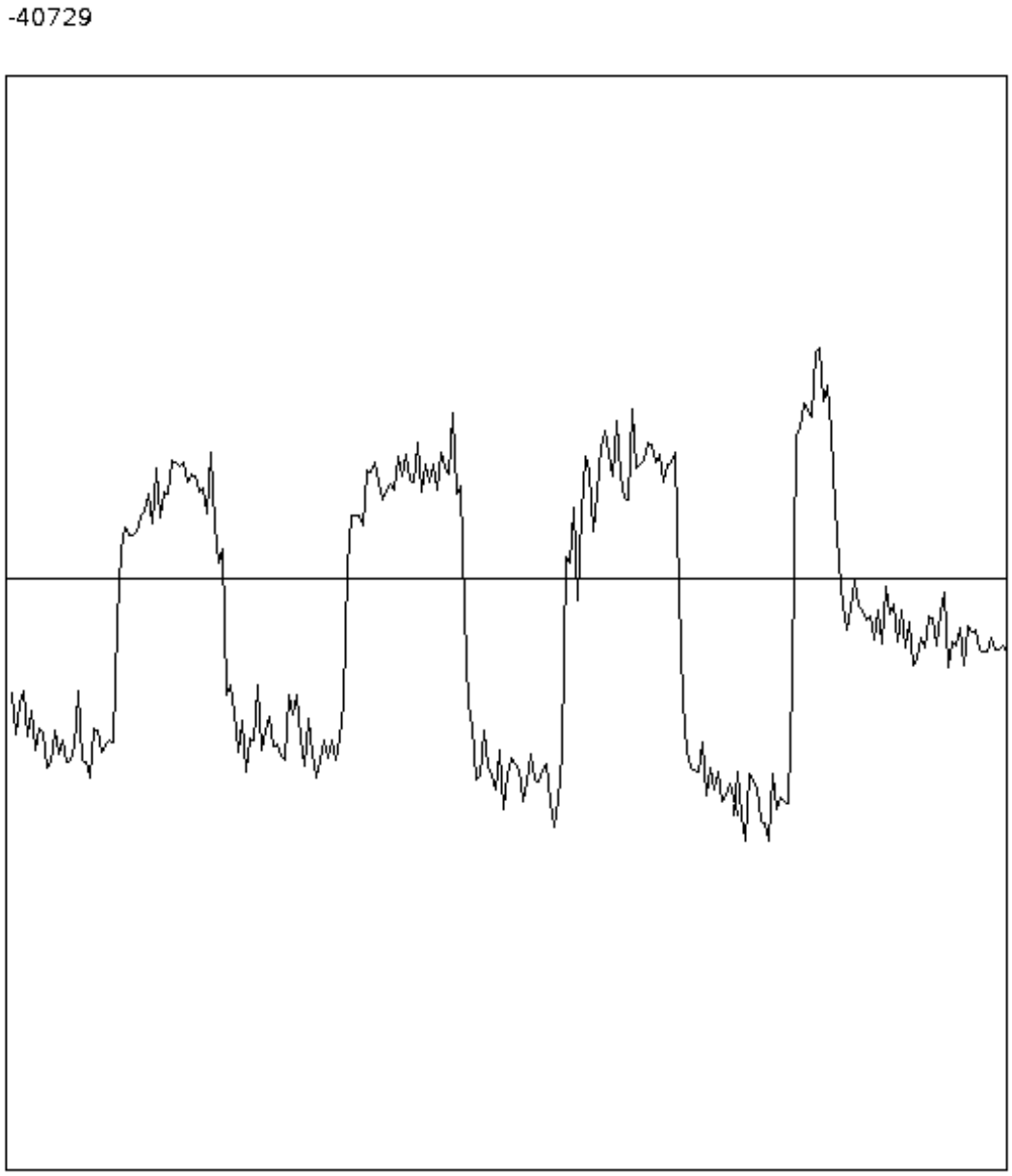

Figure 7.3: Turning a small magnet about 15 cm from the head of the sensor

We will try another test. We align the sensor in the east-west direction, null the offset and we let the sensor turn a full circle. We see we need to set the divisor at least 4. Result can be seen in figure 5.4.

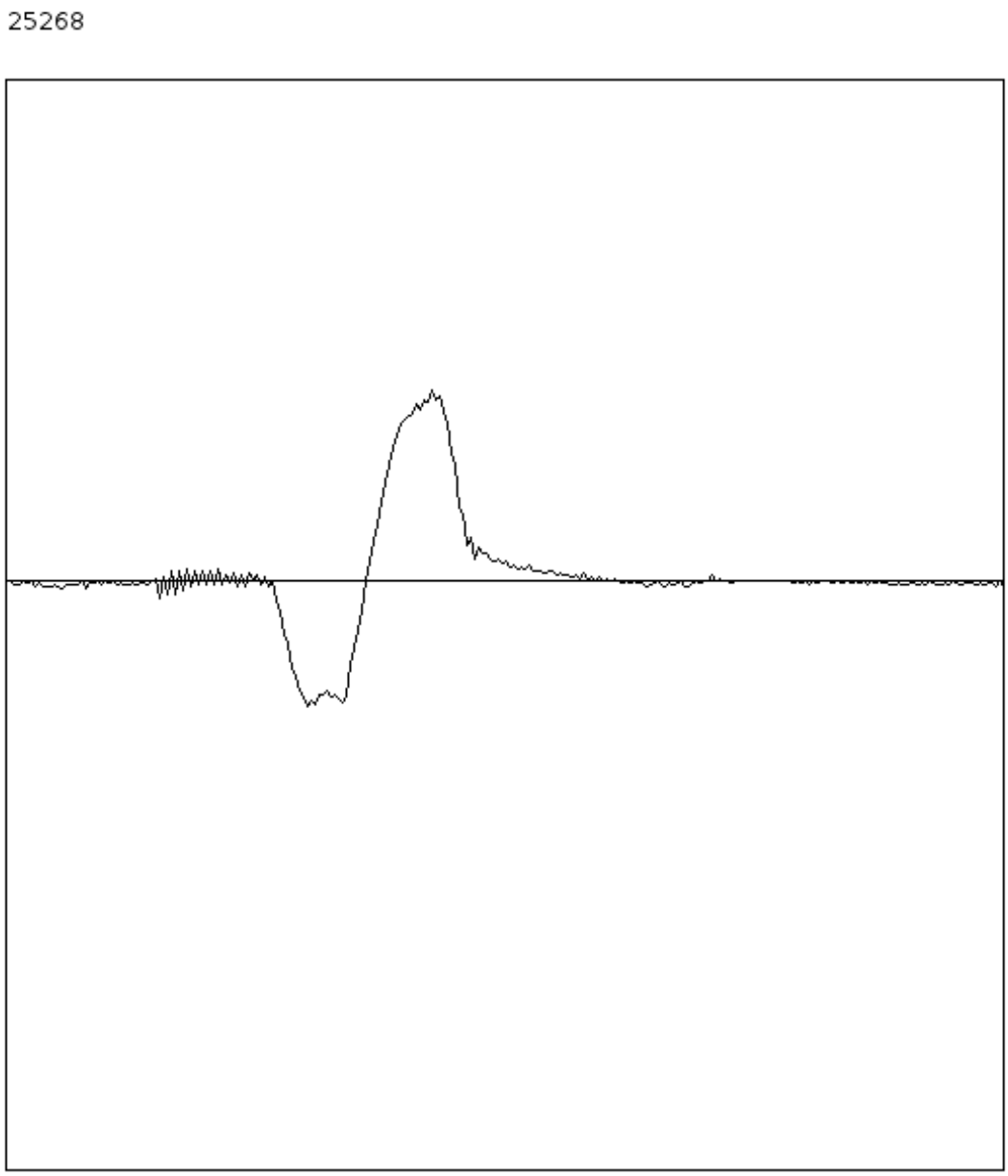

Figure 7.4: The sensor turns one full circle in horizontal plane

First practical experiments revealed an unpleasing fact: the sensor is very sensible to deformation and stress. Although it was mounted on plastic rule, any movement of whole setup brings noise to measurement and device parameters are unstable in time. See figure 7.5 where one horizontal full circle is followed by five gentle touches on sensor body. This fact forces us to develop a new sensor.

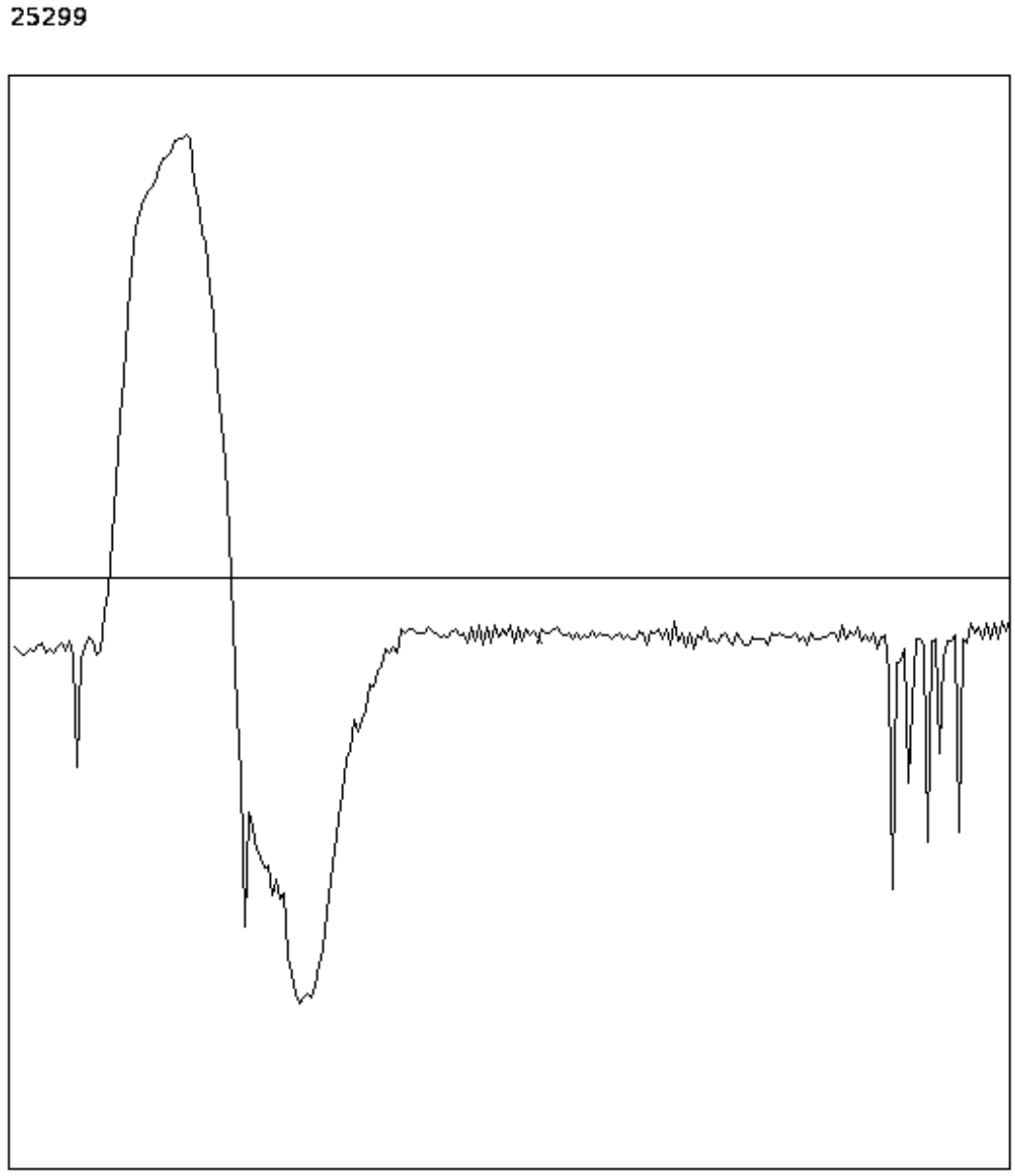

Figure 7.5: The sensor turns one full circle in horizontal plane, then it faces few soft touches on sensor body

Chapter 8

Conclusion

The first goal of my thesis, to give an explanation of the fluxgate magnetometer's operation, was done. Magnetic engineering basics were introduced and the fluxgate operation was described. The formula (4.10) for symmetrical differential sensor was derived. The second harmonic demodulation method and feedback usage were introduced. Several sensor designs were described.

The second goal, to give an overview of modern fluxgate magnetometers dedicated to space research, was completed as well. I studied fluxgate magnetometers used or proposed for Ørsted, THEMIS, Double Star, Bepi Colombo and other missions. General shift from analog to digital devices was recognized. Parameters and features of modern space-born instruments were investigated.

The third goal, to design and construct a prototype of the fluxgate magnetometer capable of measuring solar triggered activity of Earth's magnetic field, is not completely fulfilled yet. System architecture was designed. Communication, control and interface systems were successfully implemented. Simple sense and drive electronics were designed and implemented.

The sensor was manufactured from available materials. It proves correct function of all other subsystems, but the sensor instability and sensitivity to mechanical stress made measurement impossible. This failure was partially corrected by mounting the sensor on a plastic ruler. It allows some experimentation, but the sensor offset and gain is instable in time. I observed strong feed-through from the excitation winding to the sense winding. This points to the sensor asymmetry. This effect has to be examined.

New sensor has to be more stable. I will try to achieve it by a different core material and a sensor mount design. Also mechanism to adjust a possible asymmetry has to be considered. The sensor mount has to be designed with the calibration procedure in mind. Sensor input and output tuning [15] has to be surveyed. Printed circuit boards for all devices are planned to be designed and manufactured.

It is worth having detailed magnetization curves of used materials. The device for studying magnetization curves of various materials is planned to be constructed. Then the formula (4.10) can be further investigated. Work continues to have the operating device ready in September 2011.

Bibliography

[1] AUSTER et al. *The THEMIS Fluxgate Magnetometer.* Space Sci. Rev. 2008.

[2] *AVRDUDE - AVR Downloader/UploaDEr* [online]. last revision 8th of January 2010.
URL: <http://www.nongnu.org/avrdude/> [cit. 2011-7-16]

[3] *AVR Libc Home Page* [online]. last revision 16th of February 2010.
URL: <http://www.nongnu.org/avr-libc/> [cit. 2011-7-16]

[4] BROWN UNIVERSITY. *A Simple Fluxgate Magnetometer* [online]. last revision 2006. URL: <https://wiki.brown.edu/confluence/download/attachments/29069/Fluxgate+Magnetometer.pdf?version=1&modificationDate=1183038899000> [cit. 2011-7-16]

[5] CARR et al. *The Double Star magnetic field investigation: instrument design, performance and highlights of the first years observations.* Annales Geophysicae. 2005.

[6] DANMARKS METEOROLOGISKE INSTITUT. *Ørsted mission web page* [online]. last revision 4th of July 2004.
URL: <http://dmiweb.dmi.dk/fsweb/projects/oersted/> [cit. 2011-6-3]

[7] FALSTAD, Paul. *Math, Physics, and Engineering Applets* [online]. last revision date not available.
URL: <http://www.falstad.com/mathphysics.html> [cit. 2011-7-16]

[8] GLASSMEIER et al. *The Fluxgate magnetometer of the BepiColombo Mercury Planetary Orbiter.* Planet. Space Sci. 2008.

[9] MACKENZIE, David *stty man page* [online]. last revision January 2011.
URL: <http://unixhelp.ed.ac.uk/CGI/man-cgi?stty> [cit. 2011-7-16]

[10] MAUGH, Thomas. *Victor Vacquier Sr. dies at 101; geophysicist was a master of magnetics.* [online]. Los Angeles Times, January 24, 2009. URL: <http://www.latimes.com/news/science/la-me-vacquier24-2009jan24,0,3328591.story> [cit. 2011-6-3]

[11] *MLAB homepage* [online]. last revision 16th of July 2011.
URL: <http://www.mlab.cz/index.en.html> [cit. 2011-7-16]

[12] NIELSEN et al. *Development, construction and analysis of the 'Ørsted' fluxgate magnetometer.* Meas. Sci. Technol. 1995

[13] PAVELKA, Roman. *Atmel AVR development on GNU/Linux* [online]. last revision 5th December 2010.
URL: <http://kmlinux.fjfi.cvut.cz/~pavelro1/avr_tutorial.php> [cit. 2011-7-16]

[14] PRIMDAHL, Fritz. *The Fluxgate Mechanism, Part I: The Gating Curves of Parallel and Orthogonal Fluxgates.* IEEE Trans. Magn. 1970

[15] RIPKA, Pavel, *Magnetic Sensors and Magnetometers.* Artech House Publishers. ISBN-10: 1580530575. 494 p.

[16] SNARE, Robert. *A History of Vector Magnetometry in Space* [online]. last revision date not available.
URL:<http://www-ssc.igpp.ucla.edu/personnel/russell/ESS265/History.html> [cit. 2011-6-3]

[17] ŠTOLL, Ivan. *Elektřina a magnetismus.* 2nd edition. Nakladatelství ČVUT. 2003. 215 p. ISBN 80-01-02693-0.

[18] WIKIMEDIA COMMONS. *B-H Loop* [online]. last revision 20th May of 2006.
URL:
<http://en.wikipedia.org/wiki/File:B-H_loop.png> [cit. 2011-6-3]

Appendix A

Content of enclosed CD-ROM

- **firmware** Directory with the C code and Makefile of microcontroller firmware
- **logger** Directory with the C++ code and Makefile of the *logger* program
- **schematics** Directory with all used schematics
- **scope** Directory with the C++ code and Makefile of the *scope* program
- **fluxgate.pdf** This thesis in PDF format
- **fluxgate.ps** This thesis in PS format
- **stty_setting.txt** Text file with a bash command to serial port setting

Appendix B

Used software

Development

- **bash** GNU Bourne-Again SHell
- **nano** Nano's ANOther editor, an enhanced free Pico clone
- **kate** Advanced text editor for KDE
- **make** GNU make utility to maintain groups of programs
- **avr-gcc** GNU C Compiler for AVR microcontroller
- **avrdude** AVR Downloader/UploaDEr
- **gnuplot** An interactive plotting program
- **kicad** Open source software suite for electronic design automation
- **CicuitSimulator** Paul Falstadt's circuit simulation applet
- **Qt** cross-platform application framework

Publication

- **nano** Nano's ANOther editor, an enhanced free Pico clone
- **kate** Advanced text editor for KDE
- **LaTeX** Structured text formatting and typesetting system
- **pdflatex** PDF output front-end for LaTeX
- **gimp** GNU Image Manipulation Program
- **pygments** Python-based syntax highlighter